Electrical modeling of InAs/GaSb superlattice mid-wavelength infrared pin photodiode to analyze experimental dark current characteristics

Marie Delmas, Jean-Baptiste Rodriguez, and Philippe Christol

Electrical modeling of InAs/GaSb superlattice mid-wavelength infrared pin photodiode to analyze experimental dark current characteristics

Marie Delmas, Jean-Baptiste Rodriguez, and Philippe Christol
Univ. Montpellier, IES, UMR 5214, F-34000 Montpellier, France and CNRS, IES, UMR 5214, F-34000 Montpellier, France

Dark current characteristics of 7 Monolayers (ML) InAs/ 4 ML GaSb SL pin photodiodes are simulated using ATLAS software. Using appropriate models and material parameters, we obtain good agreement between the simulated and the experimental dark current curves of photodiodes grown by molecular beam epitaxy. The n-type non-intentionally-doped (nid) SL samples exhibit a dependence of the lifetime with temperature following the $T^{-\frac{1}{2}}$ law, signature of Shockley-Read-Hall (SRH) Generation-Recombination current. We also studied the dependence of the dark current with the absorber doping level. It appears that the absorber doping level must not exceed a value of $2 \times 10^{15}\,cm^{-3}$, above this value the dark current is increasing with increased doping level. However for this doping value, a dark current as low as 5×10^{-9} A/cm^2, at 50 mV reverse bias at 77 K can be obtained. © *2014 AIP Publishing LLC.* [http://dx.doi.org/10.1063/1.4895983]

I. INTRODUCTION

Since the type-II InAs/GaSb superlattice (SL) has been proposed as a material for infrared (IR) detection,[1] high performance focal plane arrays in both the mid-wavelength infrared (MWIR)[2–4] and long-wavelength infrared (LWIR)[5,6] spectral bands have been demonstrated. Thanks to the high effective mass and the band structure engineering, the tunneling currents can be reduced[1] and the Auger recombination can be suppressed[7] making the SL an alternative to mercury cadmium telluride (MCT) for IR detection.

Another advantage offered by the SL is the possibility to choose different period compositions for a given wavelength. Recent works demonstrate the strong influence of the InAs/GaSb SL period thickness and composition on both material properties and photodetector performances.[8] By the choice of an asymmetric SL period with thicker InAs layer than GaSb layer (also called InAs-rich SL structure), the dark current can be reduced by a factor 4 compared to a symmetric SL period (same InAs and GaSb layer thicknesses) having the same cut-off wavelength at 5 μm at 77 K.

In order to understand and explain the performances of the InAs-rich SL structure, we report in this paper the results of electrical modeling using the ATLAS software from SILVACO. ATLAS is a commercially available physically based device simulator often used for the simulation of III–V devices, in particular for IR detectors.[9,10] Electrical modeling with analytical expressions of the dark current components, of MWIR (Ref. 11) and LWIR (Refs. 12 and 13) SL photodiodes, has already been reported in the literature. The advantage of using ATLAS rather than analytical expressions is that by approximating the operation of a device onto a two or three dimensional grid and by applying differential equations derived from Maxwell's laws onto this grid, it can predict electrical characteristics by specifying the physicals structure at specified bias conditions. This permits to simulate more accurately the device performances and therefore not to have to approximate and derivate expressions for dark-current simulation.

The main objective of this paper is to use the simulation as a tool to understand and analyze the electrical performances of the InAs-rich SL. The model used for the simulation of the dark current-voltage (J-V) characteristics of SL photodiodes is depicted in section II- and section III- describes the InAs-rich SL structure and the associated material parameters used in ATLAS simulation. Section IV compares simulated J-V curves with experimental results obtained on non-intentionally doped (nid) and p-doped SL photodiodes fabricated by molecular beam epitaxy (MBE). The comparison allow analyzing the dark current mechanisms limiting the electrical performances of MWIR SL photodiodes.

II. MODEL FOR DARK CURRENT SIMULATION

The dark-current of an InAs/GaSb SL photodiode under moderate reverse bias is mainly limited by the generation-recombination (GR) current at low temperature and by the diffusion current at high temperature.[14] In addition, under some conditions of reverse bias and residual doping level, the trap-assisted tunneling and the band-to-band tunneling can affect the dark current.

The diffusion current contribution is due to the transport of thermally generated minority carriers from the quasi-neutral regions to the junction. It is obtained by solving the drift-diffusion model using the following expression:

$$J_{n,p} = q(n,p)\mu_{n,p}E \pm qD_{n,p}\nabla_{n,p}, \qquad (1)$$

where J represents the current density, q is the electronic charge, μ is the mobility, E is the electric field, D is the diffusion constant and n,p are the electron and hole concentration, respectively. The subscripts n and p are used to denote electron and hole components.

The generation-recombination process in the depletion region is due to the presence of traps within the forbidden

gap of the semiconductor. It is described by the Shockley-Read-Hall (SRH) recombination rate[15,16] as,

$$R_{SRH} = \frac{pn - n_i^2}{\tau_p\left[n + n_i \exp\left(\frac{E_{trap}}{kT_L}\right)\right] + \tau_n\left[p + n_i \exp\left(\frac{-E_{trap}}{kT_L}\right)\right]},$$ (2)

where n, p and n_i are the electron, the hole and the intrinsic carrier concentration, respectively. E_{trap} is the difference between the trap energy level and the intrinsic Fermi level, k is the Boltzmann constant and T_L is the lattice temperature. τ_n and τ_p are the electron and hole carrier lifetime which are set equal.

The GR current density is simply given by:

$$J_{GR} = q \int_W R_{SRH} dy,$$ (3)

with W the depletion width.

The trap-assisted tunneling (TAT) current is also modeled by including a field effect factor Γ to modify the lifetime in Eq. (2) according to Hurkx et al.[17] This field effect enhancement factor Γ includes the effect of phonon assisted tunneling on the emission of electrons and holes from a trap. The recombination rate expression becomes:

$$R_{SRH} = \frac{pn - n_i^2}{\frac{\tau_p}{1 + \Gamma_p}\left[n + n_i \exp\left(\frac{E_{trap}}{kT_L}\right)\right] + \frac{\tau_n}{1 + \Gamma_n}\left[p + n_i \exp\left(\frac{-E_{trap}}{kT_L}\right)\right]},$$ (4)

with $\Gamma_{n,p}$ the field-effect enhancement term given by:

$$\Gamma_{n,p} = \frac{\Delta E_{n,p}}{kT_L} \int_0^1 \exp\left(\frac{\Delta E_{n,p}}{kT_L}u - K_{n,p}u^{\frac{3}{2}}\right)du,$$ (5)

where $\Delta E_{n,p}$ is the energy range in which the tunneling can occur for an electron or a hole, and u is the integration variable. $K_{n,p}$ is defined as:

$$K_{n,p} = \frac{4}{3}\frac{\sqrt{2.m_t.\Delta E_{n,p}^3}}{q\frac{h}{2\pi}|E|},$$ (6)

with m_t the tunneling mass, E is the electric field and h the Plank's constant.

This approach, combining GR and TAT currents, was recently used to explain the electrical performances of LWIR unipolar SL detectors.[18]

There are two ways (local or non-local), available in ATLAS, to model the band-to-band tunneling (BTB) process. The local model calculates a recombination-generation rate at each point based solely on the value of the localized field on this point. To model the tunneling process more accurately, we used the non-local model which takes into account the spatial variation of energy bands and that the generation-recombination of opposite carrier types is not spatially coincident.

III. InAs/GaSb SL STRUCTURE AND MATERIAL PARAMETERS

The InAs/GaSb SL P-i-N structure studied in this work is depicted in Figure 1. It consists of a 200 nm thick p-doped ($P \sim 1 \times 10^{18}$ cm^{-3}) GaSb buffer layer, followed by a 60 nm thick p-doped ($P \sim 1 \times 10^{18}$ cm^{-3}) InAs/GaSb SL, a 500 nm thick non-intentionnaly doped (nid) InAs/GaSb SL active region, a 60 nm thick n-doped ($N \sim 5 \times 10^{17}$ cm^{-3}) InAs/GaSb

SL, and a 20 nm Te-doped ($N \sim 5 \times 10^{17}$ cm^{-3}) InAs contact layer. The period of the InAs/GaSb SL is composed of 7 ML of InAs and 4 ML of GaSb (InAs-rich SL). To avoid large run-times, the simulated structures have been limited to a 1 μm $\times$ 1 μm cross section while actual mesa diodes with circular cross-section of diameter from 60 μm up to 310 μm have been fabricated. Some intrinsic properties of the SLs, i.e., the electronic transport inside minibands, cannot be directly simulated by ATLAS. The material is thus defined as a bulk material, instead of a periodic stack of thin layers, with selected parameter values which are described in the next paragraph.

After defining the different regions, the material parameters for the modeling must be specified. For the two binaries,

| Cap **InAs**   n$^+$=5e17cm^{-3} (20nm) |
| 7 ML **InAs/4 GaSb**   n$^+$=5e17cm^{-3} (60nm) |
| **Active region**

7 ML **InAs/4 GaSb n.i.d** (500nm) |
| 7 ML **InAs/4 GaSb**   p$^+$=1e18cm^{-3} (60nm) |
| Buffer **GaSb**   p$^+$=1e18cm^{-3} (200nm) |

FIG. 1. Simulated SL pin structure.

InAs and GaSb, we used the values proposed by the ATLAS manual.[19] The material properties of the SL not only depend on the energy bandgap, but also on the period average composition and thickness, and it is thus difficult to draw up an exhaustive list of parameters. In the case of thick SL periods, the material can be seen as a multi-quantum well, with localized carriers having a 2D density of states. Of course, the transport modeling in these SLs must take into account all the effect due to the localization of the carriers. In our case however, the SL period is only 11 MLs thick, close to the digital alloy (about 8 MLs according to Ref. 20). We thus made the assumption that the minibands are relatively large, and that the transport properties could then be reasonably approached by defining our material as a bulk, with a 3D behavior. Some parameters were found experimentally: the SL band gap and the associated Varshni's parameters[8] were determined by photoluminescence (PL) measurement, the residual background concentration of the non-intentionally doped region was extracted from the $(A/C)^2$ curve,[21] and the type of the SL minority carriers can be assessed using Hall effect.[22] On the other hand, some physical parameters of the superlattice were calculated as a weighted average of InAs and GaSb bulk values, like the electron affinity, the permittivity, the effective mass of the holes and the electron and hole mobility. The lifetime of the minority carriers[23,24] and the effective mass of the electrons[25] were selected from the existing literature on SL MWIR photodiodes. Finally, the trap energy level and the tunneling mass were set as fitting parameters. The parameters chosen for our simulation for the InAs-rich SL are summarized in Table I.

IV. COMPARISON WITH EXPERIMENTAL RESULTS

A. Photodiodes with an undoped SL absorber layer

In order to validate the model chosen for the dark-current simulation with the defined material parameters, a set of four InAs-rich SL samples have been fabricated with a period structure close to the one depicted in the previous paragraph. They show slightly different bandgaps and background carrier concentrations, which is interesting to test the prominence of these parameters compared to the average composition. The structures were grown in a RIBER Compact 21 MBE reactor equipped with tellurium and beryllium dopant cells, and valved cracker cells for both arsenic and antimony. Photoluminescence measurements at 77 K were made on the four SL samples. Samples A and B exhibit a PL peak at 5.15 and 5.25 μm, respectively, and sample C and D at 6 μm.
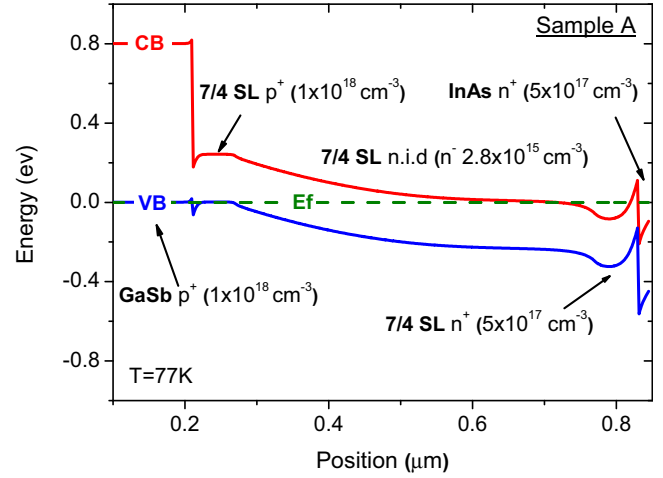

FIG. 2. Calculated energy band diagram of sample A at T = 77 K.

From epitaxial SL layers, circular mesa photodiodes were fabricated using standard photolithography and a mask-set containing diodes with several diameters from 60 up to 310 μm. CrAu was deposited as bottom and top contact metals. Mesa photodiodes were realized by wet etching, and polymerized photoresist spun onto the surface was used as a protection from ambient air. More details on the growth and the processing of the devices can be found in Refs. 26 and 27.

Capacitance-voltage (C-V) measurements were performed in order to accurately determine the n-type residual background concentration of the undoped SL. We found 2.80×10^{15}, 6×10^{15}, 1.40×10^{15}, and 3.50×10^{15} cm^{-3} for samples A, B, C, and D, respectively. The band diagram of the sample A was simulated at 77 K with the experimental values for the band gap and the residual doping (Figure 2).

The model described in Sec. II was used with m_t and E_{trap} as fitting parameters, the J-V curves were simulated at 77 K with the values summarized in Table II. Note that regarding the SRH recombination expression (Eq. (4)) there are mathematically several solution (τ_{SRH}; E_{trap}; m_t) satisfying the equation. In order to select the more realistic parameters, the lifetime was fixed to 100 ns as reported in the recent literature for similar SL material[23,24] and the corresponding energy level was found to fit the experimental data. The tunneling mass, which plays an important role on the apparition of the tunneling process, was determined first to fit the experimental curve at high reverse bias.

Results are shown in Figure 3 and compared with experimental curves. We observe a good agreement between the experimental data and simulation which demonstrates the model accuracy. We can see from Table II that the tunneling mass

TABLE I. Parameter values used for InAs-rich SL in Atlas simulation.

Parameter	Values
Permittivity	15.34 ε_0
Electron affinity	4.73 eV
Electron effective mass	$m_e = 0.0254\ m_0$
Hole effective mass	$m_h = 0.245\ m_0$
Electron mobility	2.6×10^4 cm^2/V-s
Hole mobility	680 cm^2/V-s
Lifetime (T = 77 K)	100 ns

TABLE II. Simulation parameters of samples A, B, C, and D.

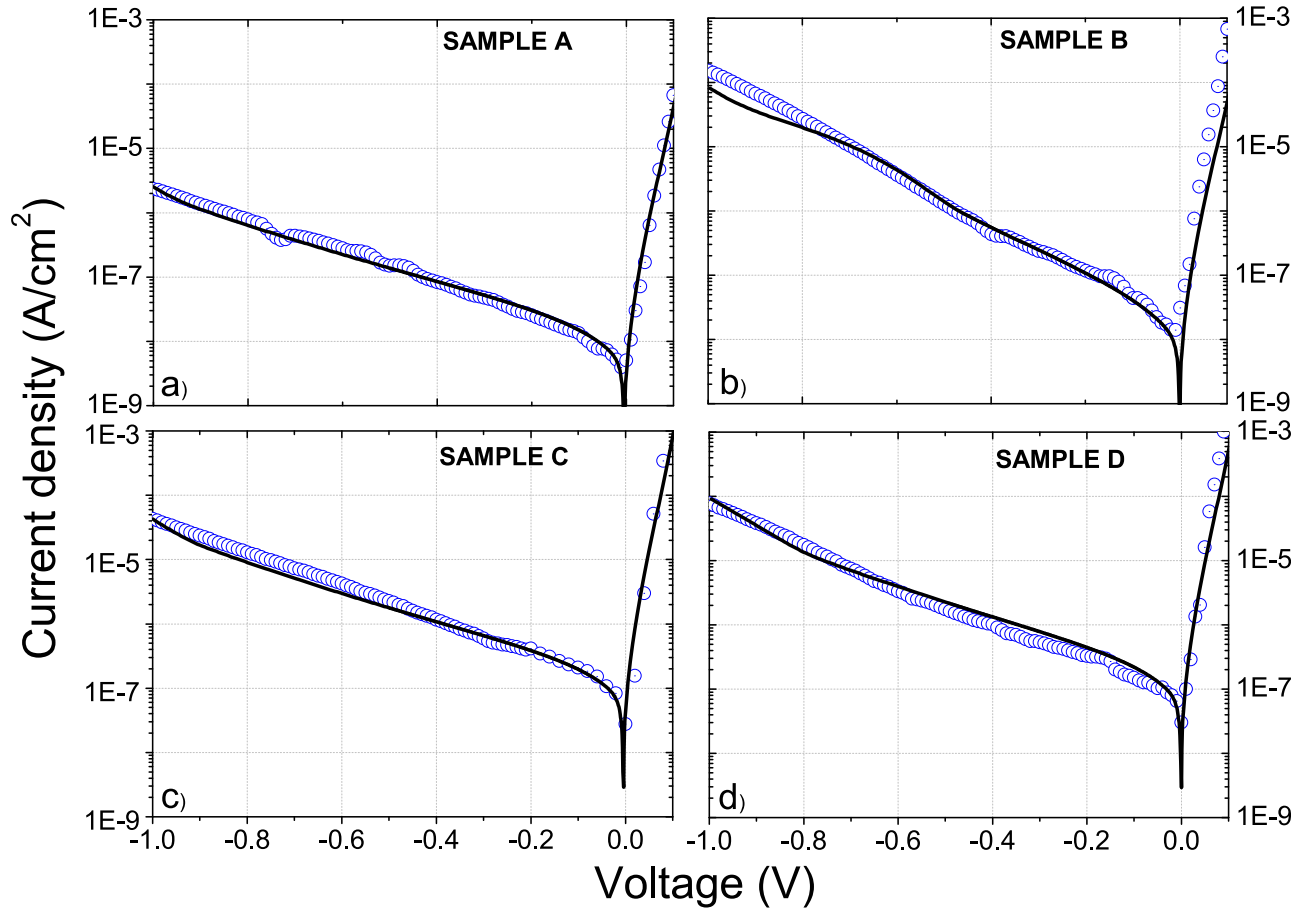| Sample	PL peak @77 K (μm)	Residual background concentration (cm^{-3})	m_t	E_{trap} (meV)
A	5.15	2.80×10^{15}	0.025	18
B	5.25	6×10^{15}	0.021	18
C	6	1.40×10^{15}	0.022	18
D	6	3.50×10^{15}	0.021	18

FIG. 3. Experimental (open circles) and simulated (solid line) J-V curves of samples A (a), B (b), C (c), and D (d) at T = 77 K.

is closed to the calculated SL reduced mass ($\frac{1}{m_t} = \frac{1}{m_e} + \frac{1}{m_h}$; $m_t = 0.023$) and appears mostly independent on the wavelength and the residual background concentration. We also found that the trap energy level is the same for the four photodiodes, located 18 meV away from the intrinsic Fermi level.

The simulation of J-V curves at different temperatures was also performed. The experimental and the simulated J-V curves for sample A are plotted in Figure 4, together with the variation of the dark-current density at −50 mV. m_t and E_{trap}

were kept constant, while the minority carrier lifetime was adjusted to fit the measurements. Figure 5 represents the lifetime values found for the simulation, as a function of temperature. Values between 100 ns and 50 ns are obtained in the 77 to 230 K temperature range. The variation of the lifetime follows a $T^{-\frac{1}{2}}$ law, which is the signature that SRH generation is the physical mechanism limiting the lifetime, as already experimentally observed on LWIR InAs/GaSb SL by Connelly *et al.*[28] This result also confirms the precision of the model and of the fitting parameters used.
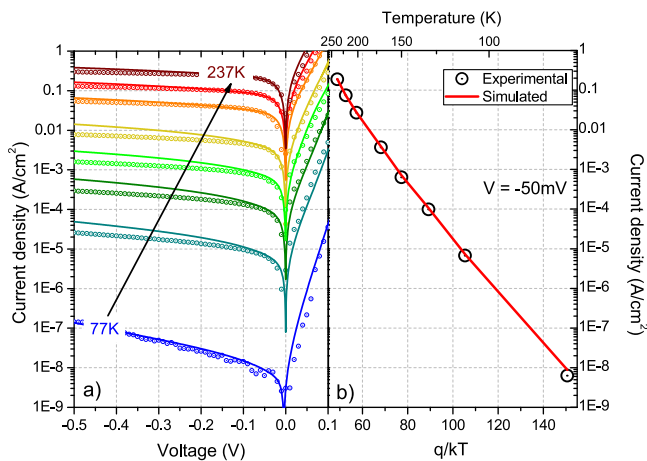

FIG. 4. (a) Experimental (open circles) and simulated J-V curves (line) of sample A at different temperatures. (b) Experimental (open circles) and simulated (line) current densities at −50 mV as a function of temperature.
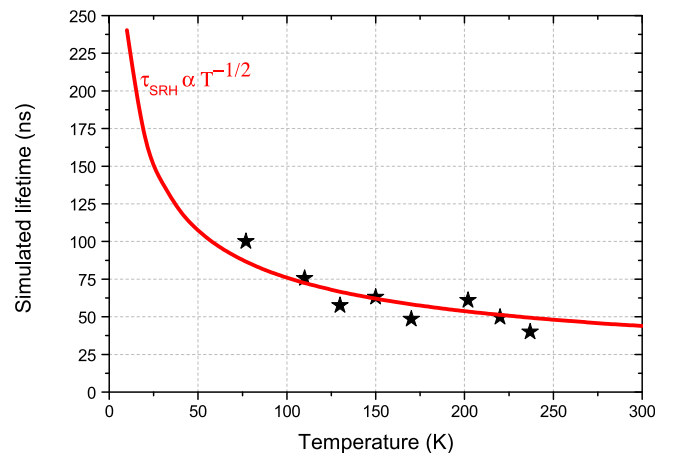

FIG. 5. Simulated lifetime as a function of temperature (stars) and the adjusted $T^{-\frac{1}{2}}$ law (solid line).

B. Photodiodes with a doped SL absorber layer

It has already been shown that by changing the n-type polarity to p-type of the SL, higher quantum efficiency can be achieved thanks to the longer diffusion length when the minority carriers are the electrons.[29] In addition, by increasing the doping level of the absorber layer, the GR current can be reduced, because it is proportional to $1/\sqrt{N}$ (with N the doping level). However, increasing the doping level also results in larger tunneling currents due to the increase of the electric field which may become dominant at some point.[28] Determining the optimum doping level is thus crucial. In order to study the effect of the absorber doping level on the electrical performances and material properties, three InAs-rich SL samples have been grown, with the same structure already depicted in Sec. III, except for the absorber layer which is intentionally doped with beryllium.

The three samples exhibit, at 77 K, PL peaks at 5.35, 5.45, and 5.35 μm for samples E, F, and G, respectively. The measured carrier concentration at 77 K is 5.8×10^{15} cm^{-3}, 1 $\times 10^{16}$ cm^{-3}, and 4.7×10^{16} cm^{-3} for samples E, F, and G, respectively. For the three structures, the simulated band-diagram and electric field at 77 K are shown in Figure 6. The electric field becomes stronger with increased doping level of the absorber region. This explains the stronger band-to-band tunneling as illustrated in Figure 7 showing the 77K J-V curves for the three devices. The simulated BTB has not exactly the same shape that the experimental curve in particular for the two most doped samples, which may demonstrate the limit of simulating the SL quantum structure as if it were a bulk material. However, it is to be noted that we can accurately predict the bias at which it starts being the dominant process. Moreover, the fitting parameters used are similar with those found previously, indicating their accuracy to describe the InAs-rich SL even though the absorber doping level and type have been changed.

In Figure 7, we can see that the dark current is degraded when the doping level of the active region is increased. In order to explain this result, the GR-TAT current and the BTB current at -50 mV at T $= 77$ K as a function of the doping level (p-type) and for two different absorber thicknesses, 500 nm and 4 μm, have been simulated using the same
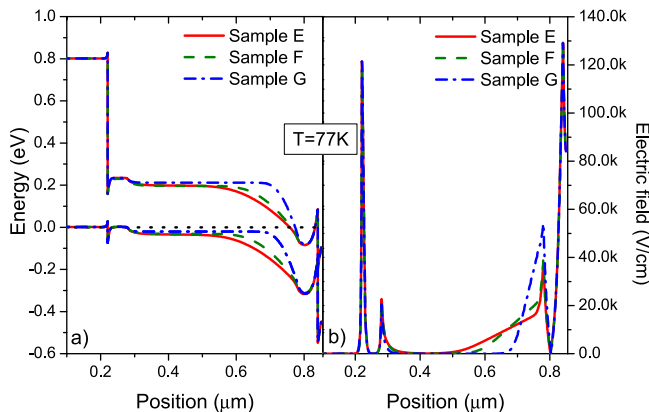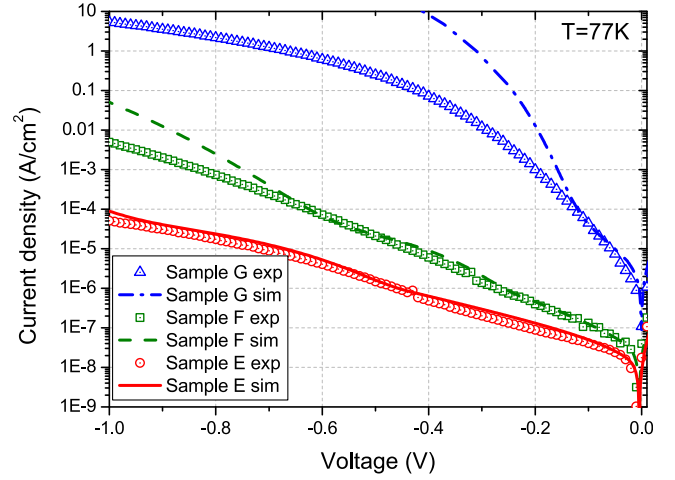

FIG. 7. Experimental (symbols) and simulated (lines) J-V curves at T $= 77$ K of samples E, F, and G.

structure that the one described in Sec. III with a cut-off wavelength of 5 μm at 77 K.

For the sake of comparison, the experimental dark current values at -50 mV were estimated for a cut-off wavelength of 5 μm using the standard analytical relationship between the GR current and the bandgap. The resulting data for the undoped (A, B, C, and D) and p-type doped samples (E, F, and G) are also plotted on Figure 8. The configuration is different between the two sets of samples, the n.i.d samples have the P-N junction on the GaSb contact layer side (at the bottom of the structure), while it is on the InAs contact layer side for the intentionally p-type doped samples. However, in both cases, one can consider it is a P-N homo-junction between the absorber and a highly doped SL, and despite the fact that the contact doping level for the N-side (5×10^{17} cm^{-3}) and the P-side (1×10^{18} cm^{-3}) is different, the dark current for the undoped and the doped samples can be compared. Indeed, the doping level of the N and P contact is much higher than that of the active region; it thus has a negligible impact on the current density.

FIG. 6. Simulated band diagram (a) and electric field (b) at 0 V at T $= 77$ K of samples E, F, and G.
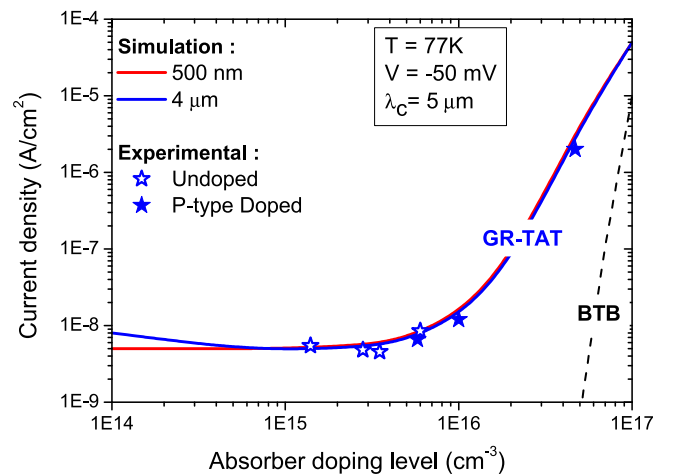

FIG. 8. Simulated BTB current (dashed line) and GR-TAT current (solid line) as a function of the absorber doping level for two different thicknesses 500 nm (red line) and 4 μm (blue line). Experimental dark current of the undoped (empty stars) and the p-type doped samples (full stars).

In the $1 \times 10^{14} \, \text{cm}^{-3}$ to $2 \times 10^{15} \, \text{cm}^{-3}$ range, the thinner structure is totally depleted ($W > 500 \, \text{nm}$), and the GR-TAT current is therefore constant. The depleted region is however still thinner than $4 \, \mu\text{m}$, and the GR-TAT current for the thicker sample thus follows the classical $1/\sqrt{N}$ law and therefore increases with decreasing carrier concentration. However, above this range, the GR-TAT current is increasing with the doping level. Indeed, the field effect factor, defined in Sec. II, becomes much higher and therefore the minority carrier lifetime is modified ($\tau = \frac{\tau_{SRH}}{1+\Gamma}$ with τ_{SRH} constant with the doping level). In addition, the band-to-band-tunneling contribution at $-50 \, \text{mV}$ is not predominant below $1 \times 10^{17} \, \text{cm}^{-3}$.

From the discussion above, it is therefore clear that improving the electrical performances of this pin SL structure cannot be achieved by doping the absorber above $2 \times 10^{15} \, \text{cm}^{-3}$. The design has to be modified using a structure keeping the absorber in flat band condition, with majority carrier blocking layers[24] or using heterostructures with large bandgap material in the high electric field region. In this configuration, GR-TAT and BTB current can be greatly reduced, and an increased doping level directly results in an improved dark-current through the reduction of the diffusion of the minority carriers. It is however important to highlight that, despite the relatively low minority carrier lifetime and carrier concentration, a dark current, at $50 \, \text{mV}$ reverse bias at $77 \, \text{K}$, comprised between $5 \times 10^{-9} \, \text{A/cm}^2$ and $8.5 \times 10^{-9} \, \text{A/cm}^2$ is obtained for doping concentration in the range of $7 \times 10^{14} \, \text{cm}^{-3}$ and $7 \times 10^{15} \, \text{cm}^{-3}$.

V. CONCLUSION

In conclusion, a set of several InAs-rich SLs photodiodes have been fabricated and modeled using ATLAS software from SILVACO. By modeling the different contributions of the dark current, we found a tunneling mass m_t around 0.023 and a trap level located at $18 \, \text{meV}$ from the intrinsic Fermi level. Keeping m_t and E_{trap} constant, we then studied the temperature dependence of the lifetime. The simulated lifetime follows a $T^{\frac{-1}{2}}$ law which is the signature of an SRH mechanism-limited lifetime. By switching the n-type polarity of the undoped InAs-rich SL samples to p-type, the fitting parameters could be kept the same, demonstrating the good accuracy of the model and the parameters used. The dark current as a function of the absorber doping level was also studied. It was shown that for a photodiode with a cut-off wavelength at $5 \, \mu\text{m}$ at $77 \, \text{K}$, the dark current increases for doping levels above $2 \times 10^{15} \, \text{cm}^{-3}$. However, a current density as low as $5 \times 10^{-9} \, \text{A/cm}^2$ for an absorber doping level close to $2 \times 10^{15} \, \text{cm}^{-3}$ was demonstrated.

ACKNOWLEDGMENTS

[1]D. L. Smith and C. Mailhiot, "Proposal for strained type II superlattice infrared detectors," J. Appl. Phys. **62**, 2545 (1987).
[2]J. W. Little, S. P. Svensson, W. A. Beck, A. C. Goldberg, S. W. Kennerly, T. Hongsmatip, M. Winn, and P. Uppal, "Thin active region, type II superlattice photodiode arrays: Single-pixel and focal plane array characterization," J. Appl. Phys. **101**, 044514 (2007).
[3]S. Abdollahi Pour, E. K. Huang, G. Chen, A. Haddadi, B.-M. Nguyen, and M. Razeghi, "High operating temperature midwave infrared photodiodes and focal plane arrays based on type-II InAs/GaSb superlattices," Appl. Phys. Lett. **98**, 143501 (2011).
[4]F. Rutz, R. Rehm, M. Walther, J. Schmitz, L. Kirste, A. Wörl, J.-M. Masur, R. Scheibner, and J. Ziegler, "InAs/GaSb superlattice technology", Inf. Phys. Technol. **54**, 237 (2011).
[5]P. Manurkar, S. Ramezani-Darvish, B.-M. Nguyen, M. Razeghi, and J. Hubbs, "High performance long wavelength infrared mega-pixel focal plane array based on type-II superlattices," Appl. Phys. Lett. **97**, 193505 (2010).
[6]A. D. Hood, A. J. Evans, A. Lkhlassi, D. L. Lee, and W. E. Tennant, "LWIR strained-layer superlattice materials and devices at Teledyne imaging sensors," J. Electron. Mater. **39**, 1001–1006 (2010).
[7]H. Mohseni, V. Litvinov, and M. Razeghi, "Interface-induced suppression of the Auger recombination in type-II InAs/GaSb superlattices," Phys. Rev. B **58**, 15378–15380 (1998).
[8]R. Taalat, J. B. Rodriguez, M. Delmas, and P. Christol, "Influence of the period thickness and composition on the electro-optical properties of type-II InAs/GaSb midwave infrared superlattice photodetectors," J. Phys. D: App. Phys **47**, 015101 (2014).
[9]K. Banerjee, J. Huang, and S. Ghosh, "Modeling and simulation of long-wave infrared InAs/GaSb strained layer superlattice photodiodes with different passivants," Inf. Phys. Technol. **54**, 460–464 (2011).
[10]J. Abautret, J. P. Perez, A. Evirgen, F. Martinez, P. Christol et al., "Electrical modeling of InSb PiN photodiode for avalanche operation," J. Appl. Phys. **113**, 183716 (2013).
[11]V. Gopal, E. Plis, C. E. Jones, L. Faraone, and S. Krishna, "Modeling of electrical characteristics of midwave type II InAs/GaSb strain layer superlattice diodes," J. Appl. Phys. **104**, 124506 (2008).
[12]Q. K. Yang, F. Fuchs, J. Schmitz, and W. Pletschen, "Investigation of trap-assisted tunneling current in InAs/(GaIn)Sb superlattice long-wavelength photodiodes," Appl. Phys. Lett. **81**, 4757 (2002).
[13]J. Nguyen, D. Z. Ting, C. J. Hill, A. Soibel, S. A. Keo, and S. D. Gunapala, "Dark current analysis of InAs/GaSb superlattices at low temperatures," Inf. Phys. Technol. **52**, 317 (2009).
[14]J. B. Rodriguez, C. Cervera, and P. Christol, "A type-II superlattice period with a modified InAs to GaSb thickness ratio for midwavelength infrared photodiode performance improvement," Appl. Phys. Lett. **97**, 251113 (2010).
[15]W. Shockley and W. T. Read, "Statistics of the recombination of holes and electrons," Phys. Rev. **87**, 835 (1952).
[16]R. N. Hall, "Electron-hole recombination in Germanium," Phys. Rev. **87**, 387 (1952).
[17]G. A. M. Hurkx, H. C. Degraff, W. J. Kloosterman, and M. P. G. Knuvers, "A new analytical diode model including tunneling and avalanche breakdown," IEEE Trans. Electron Devices **39**, 2090 (1992).
[18]F. Callewaert, A. M. Hoang, and M. Razeghi, "Generation-recombination and trap-assisted tunneling in long wavelength infrared minority electron unipolar photodetectors based on InAs/GaSb superlattice," Appl. Phys. Lett. **104**, 053508 (2014).
[19]See https://dynamic.silvaco.com/dynamicweb/jsp/downloads/Download ManualsAction.do?req=silen-manuals&name=atlas for Silvaco ATLAS Users Manual.
[20]R. Kaspi and G. P. Donati, "Digital alloy growth in mixed As/Sb heterostructures," J. Cryst. Growth **251**, 515–520 (2003).
[21]C. Cervera, J. B. Rodriguez, R. Chaghi, H. Aït-Kaci, and P. Christol, "Characterization of midwave infrared InAs/GaSb superlattice photodiode," J. Appl. Phys. **106**, 024501 (2009).
[22]C. Cervera, J. B. Rodriguez, J. P. Perez, H. Aït-Kaci, R. Chaghi, L. Konczewicz, S. Contreras, and P. Christol, "Unambiguous determination of carrier concentration and mobility for InAs/GaSb superlattice photodiode optimization," J. Appl. Phys. **106**, 033709 (2009).
[23]S. P. Svensson, D. Donetsky, D. Wang, H. Hier, F. J. Crowne, and G. Belenky, "Growth of type II strained layer superlattice, bulk InAs and GaSb materials for minority lifetime characterization," J. Cryst. Growth **334**, 103–107 (2011).
[24]L. M. Murray, K. S. Lokovic, B. V. Olson, A. Yildirim, T. F. Boggess, and J. P. Prineas, "Effects of growth rate variations on carrier lifetime and interface structure in InAs/GaSb superlattices," J. Cryst. Growth **386**, 194 (2014).
[25]B. M. Nguyen, D. Hoffman, P. Y. Delaunay, E.-K. Huang, and M. Razeghi, "Very high performance LWIR and VLWIR Type-II InAs/GaSb superlattice photodiodes with M-structure barrier," Proc. SPIE **7082**, 708205 (2008).

[26]J. B. Rodriguez, P. Christol, L. Cerutti, F. Chevrier, and A. Joullié, "MBE growth and characterization of type-II InAs/GaSb superlattices for mid-infrared detection," J. Cryst. Growth **274**, 6–13 (2005).

[27]R. Chaghi, C. Cervera, H. Aït-Kaci, P. Grech, J. B. Rodriguez, and P. Christol, "Wet etching and chemical polishing of InAs/GaSb superlattice photodiodes," Semicond. Sci. Technol. **24**, 065010 (2009).

[28]B. C. Connelly, G. D. Metcalfe, H. Shen, and M. Wraback, "Direct minority carrier lifetime measurements and recombination mechanisms in long-wave infrared type II superlattices using time-resolved photoluminescence," Appl. Phys. Lett. **97**, 251117 (2010).

[29]D. Hoffman, B.-M. Nguyen, P.-Y. Delaunay, A. Hood, M. Razeghi, and J. Pellegrin, "Beryllium compensation doping of InAs/GaSb infrared superlattice photodiodes," Appl. Phys. Lett. **91**, 143507 (2007).